Seasonal and interannual variations in the surface energy fluxes of a rice–wheat rotation in Eastern China

Article

Accepted Version

Duan, Z., Grimmond, S. ORCID: https://orcid.org/0000-0002-3166-9415, Gao, C. Y., Sun, T. ORCID: https://orcid.org/0000-0002-2486-6146, Liu, C., Wang, L., Li, Y. and Gao, Z. (2021) Seasonal and interannual variations in the surface energy fluxes of a rice–wheat rotation in Eastern China. Journal of Applied Meteorology and Climatology, 60 (7). pp. 877-891. ISSN 1558-8432 doi: 10.1175/jamc-d-20-0233.1 Available at https://centaur.reading.ac.uk/98435/

To link to this article DOI: http://dx.doi.org/10.1175/jamc-d-20-0233.1

Publisher: American Meteorological Society

Seasonal and interannual variations in the surface energy fluxes of a rice–wheat rotation in Eastern China

Zexia Duan [a], C S B Grimmond [b], Chloe Y. Gao [c], Ting Sun [b], Changwei Liu [a], Linlin Wang [c], Yubin Li [a], and Zhiqiu Gao [a,d]

[a] *Climate and Weather Disasters Collaborative Innovation Center, School of Atmospheric Physics, Nanjing University of Information Science and Technology, Nanjing, 210044, China*

[b] *Department of Meteorology, University of Reading, Reading, RG6 6ET, United Kingdom*

[c] *Program in Atmospheric and Oceanic Sciences, Princeton University, Princeton, NJ, 08544, United States*

[d] *State Key Laboratory of Atmospheric Boundary Layer Physics and Atmospheric Chemistry, Institute of Atmospheric Physics, Chinese Academy of Sciences, Beijing, 100029, China*

Corresponding author: Dr. Zhiqiu Gao, zgao@mail.iap.ac.cn

Early Online Release: This preliminary version has been accepted for publication in *Journal of Applied Meteorology and Climatology*, may be fully cited, and has been assigned DOI 10.1175/JAMC-D-20-0233.1. The final typeset copyedited article will replace the EOR at the above DOI when it is published.

ABSTRACT

Quantitative knowledge of the water and energy exchanges in agroecosystems is vital for irrigation management and modeling crop production. In this study, the seasonal and annual variabilities of evapotranspiration (*ET*) and energy exchanges were investigated under two different crop environments – flooded and aerobic soil conditions – using three years (June 2014 to May 2017) of eddy covariance observations over a rice–wheat rotation in eastern China. Across the whole rice-wheat rotation, the average daily *ET* rate in the rice paddies and wheat fields was 3.6 mm d^{-1} and 2.4 mm d^{-1}, respectively. The average seasonal *ET* was 473 and 387 mm for rice and wheat fields, indicating a higher water consumption for rice than for wheat. Averaging for the three cropping seasons, rice paddies had 52% more latent heat flux than wheat fields, whereas wheat had 73% more sensible heat flux than rice paddies. This resulted in a lower Bowen ratio in the rice paddies (0.14) than in the wheat fields (0.4). As eddy covariance observations of turbulent heat fluxes are typically less than the available energy ($R_n - G$, i.e., net radiation minus soil heat flux), energy balance closure (EBC) therefore does not occur. For rice, EBC was greatest at the vegetative growth stages (mean: 0.90) after considering the water heat storage, whereas wheat had its best EBC at the ripening stages (mean: 0.86).

1. Introduction

Land–atmosphere exchanges of energy and mass play a crucial role in hydrological, climatological and biological processes (You et al., 2017). Our

Accepted for publication in *Journal of Applied Meteorology and Climatology*. DOI 10.1175/JAMC-D-20-0233.1.

understanding of these processes largely relies on observations from eddy covariance (EC) flux measurement towers (Stoy et al., 2013). The EC technique is considered to be the most direct and trustworthy method to monitor soil–plant–atmosphere carbon, water, and energy fluxes (Baldocchi, 2003).

Many meteorological and air-quality models are especially sensitive to the seasonal variations in surface energy partitioning of available energy into sensible heat flux (H) and latent heat flux (λET) (Bi et al., 2007; Hossen et al., 2012). Based on successive EC measurements of water and energy fluxes, seasonal and interannual energy partitioning and evapotranspiration (ET) in agricultural areas have considered winter wheat (Schmidt et al., 2012; Eshonkulov et al., 2019), winter wheat/summer maize rotation cropland (Lei and Yang, 2010), cotton (Oncley et al., 2007), and rice paddies (Gao et al., 2003; Tsai et al., 2007; Alberto et al., 2009; Hossen et al., 2012; Timm et al., 2014; Masseroni et al., 2015). Previous studies have reported that the partitioning of the net radiation (R_n) into λET, H and soil heat flux (G) is closely related to meteorological factors (e.g., solar radiation, temperature, and moisture) and biological factors (e.g., plant functional type, phenology, and stomatal regulation) (Ding et al., 2013; Jia et al., 2016). In recent decades, intense human activities and agronomic measures (e.g., irrigation methods, crop rotation, and changes in soil fertility) have dramatically affected the ecological and hydrological processes of agricultural areas, including energy partitioning, aerodynamic characteristics, soil water content, ET and carbon sequestration (Liu et al., 2019). Despite efforts to investigate the surface

Accepted for publication in *Journal of Applied Meteorology and Climatology*. DOI 10.1175/JAMC-D-20-0233.1.

partitioning of the available energy into H and λET, there is still considerable uncertainty regarding the magnitude of the energy fluxes from rice–wheat rotation ecosystems in eastern China.

Rice–wheat rotation, with two crops per year, increases crop yield and land-use efficiency (Lan et al., 2020). This ubiquitous rotation in East and Southeast Asia (e.g., India, Nepal, China), covering ~26 million hectares (Timsina and Connor, 2001), provides a stable food source for more than 20% of the world's population (Kumari et al., 2011). Thus, it is significant to regional and global food security (Jin et al., 2020). Surface–atmosphere exchanges differ between rice paddies and wheat because of the paddy water regime. The common practice for rice involves flooding the field, alternating with mid-season aeration, and draining before harvest; whereas for wheat, a regime of trenching and draining is used to prevent flood damage (Zhao et al., 2009). The unique water management scheme with several dry–wet cycles causes large changes in ET and energy partitioning during the two crop seasons.

Hence, exploring these ET and energy partitioning variations is important for a better understanding of regional climate, irrigation scheduling, and modeling crop production (Ma et al., 2015; Yan et al., 2015). In the present work, a rice–wheat crop rotation in eastern China was studied using three years of heat and water EC flux measurements. The objectives were to: (1) quantify the seasonal and interannual variations in surface heat fluxes (radiative, turbulent, and ground heat) to characterize the differences between the rice and wheat growing seasons; and (2) explore the

Accepted for publication in *Journal of Applied Meteorology and Climatology*. DOI 10.1175/JAMC-D-20-0233.1.

dynamics of *ET*, energy partitioning and energy closure over the rice–wheat rotation cropland.

2. Methods

a. Study site

A 300 m × 300 m site in Dongtai County, Jiangsu Province, China (Figure 1a; 32.76°N, 120.47°E; 4 m above sea level), situated approximately 45 km west of the East China Sea, was used in this study. The subtropical monsoon climate has a mean annual (1984–2013) air temperature of 15.1 ± 0.61°C and precipitation of 1060 ± 268 mm (WMO station: 58251 Dongtai Station; Ge et al., 2018).

The site is relatively flat, with predominantly clay soils. Summer rice paddy and winter wheat grew in the fetch of the EC instruments (90% probable footprint; Section 2d). Three crop years (2014–15, 2015–16, and 2016–17) were studied, each with a rotation of summer rice and winter wheat cultivated in the field around the EC tower (Section 2b).

For rice cultivation (Table 1) the field was prepared in early June by flooding, plowing, and harrowing to incorporate the wheat straw residue from the previous wheat crop prior to the field being levelled. A local mid-season japonica rice cultivar (Huaidao 5) was sown in the seed bed in mid-May. In mid-June, 30-day-old seedlings were transplanted using a mechanical transplanter with a spacing of 0.25 m × 0.13 m. Nitrogen fertilizer (urea) was applied at a rate of 200 kg ha^{-1} for the rice growing

Accepted for publication in *Journal of Applied Meteorology and Climatology*. DOI 10.1175/JAMC-D-20-0233.1.

season. The ~150-day rice growing season had three stages: vegetative (Figure 1c), reproductive (Figure 1d), and ripening (Figure 1e) (South Shen Zao Zhen: local agrotechnical station, personal communication 2018). At the beginning of the vegetative stage, the rice field was kept saturated but not flooded, to allow the rice seedlings to recover from transplantation shock. Then, the rice field was kept flooded with 0.15 ± 0.05 m of standing water until late August. Afterwards, the field was flooded intermittently (water depth: ~0.05 m) until five weeks before harvest. Finally, the floodwater was naturally drained from the field until the harvest in mid-November. The irrigation water was from the surrounding rivers.

The 200-day "Yangmai 16" variety winter wheat growth period extended from late November sowing to harvest in late May the next year (Table 1). Nitrogen fertilizer (urea) was applied at a rate of 180 kg ha^{-1}. The three growth stages were related to wheat phenology: vegetative (Figure 1f), reproductive (Figure 1g), and ripening (Figure 1h). Wheat was directly seeded in well-drained and non-puddled soils, and grew under unsaturated soil moisture conditions during most crop growth periods. The combine harvester, used for both crops, left all the rice straw and wheat residues on the field.

b. Instruments and data processing

The EC technique (Figure 1b) allows scalar fluxes to be measured within the atmospheric surface layer, enabling quasi-continuous long-term measurements with minimal disturbance to the ecosystem. For this study, a three-dimensional sonic

Accepted for publication in *Journal of Applied Meteorology and Climatology*. DOI 10.1175/JAMC-D-20-0233.1.

anemometer (CSAT3, Campbell Scientific Inc., Logan, UT, USA) and a CO_2/H_2O open-path gas analyzer (LI-7500, LI-COR, Biosciences Inc., Lincoln, NE, USA) were mounted 10 m above ground level (agl) and sampled at 10 Hz.

Other sensors measured air temperature and humidity (HMP45A, Vaisala, Finland), wind speed and wind direction (034B, Met One Inc., USA), all at 3, 5, 8 and 10 m agl, and a 4-component net radiometer (CNR-4, Kipp & Zonen Inc., Netherlands) was at 3 m agl. These variables were sampled at 1 Hz using a CR3000 datalogger (Campbell Scientific, Inc., USA) and averaged to 30 min. The *G* (using HFP01 heat flux plates, Hukseflux Thermal Sensors, Delft, Netherlands), soil temperature (PT100, Campbell Scientific, Inc., USA), and soil water content (CS616, Campbell Scientific, Inc., USA) were measured at 0.05, 0.1, 0.2 and 0.4 m below the ground surface. Additionally, surface atmospheric pressure (PTB110, Vaisala, Inc., Finland) and precipitation (TE525MM, Campbell Scientific, Inc., USA) were observed. More details about the instruments can be found in Li et al. (2017).

The raw 10 Hz EC data were obtained with the LoggerNet 4.2.1 (Campbell Scientific, Inc., 2013) software and transformed into 30 min binaries. These were processed using EddyPro 5.2.1 (LI-COR Inc., 2015) software into half-hourly fluxes. The data processing included: averaging and statistical tests (Lee et al., 2004); time lag compensation; double rotation for tilt correction; spectral corrections (Moncrieff et al., 2004); and compensation for density fluctuations (Webb et al., 1980). The EddyPro quality flags ranged from 'best' (0) to 'suitable for general analysis' (e.g., annual

Accepted for publication in *Journal of Applied Meteorology and Climatology*. DOI 10.1175/JAMC-D-20-0233.1.

budgets) (1) to ‘discard’ (2). As EC systems are unable to measure in rainy or foggy conditions, data collected under such conditions were excluded. Other data losses occurred when switching data storage cards and power outages (e.g., large data gap in 2017).

The 8-day leaf area index (*LAI*) data from June 2014 to May 2017 were from the MODIS MOD15A2H with 500-m resolution. This MODIS data can be downloaded from https://lpdaac.usgs.gov, maintained by the NASA EOSDIS Land Processes Distributed Active Archive Center (LP DAAC) at the USGS Earth Resources Observation and Science (EROS) Center.

c. Radiation and surface energy fluxes

When the storage heat flux of the canopy is not explicitly addressed, the surface energy balance for a crop canopy can be written (Burba et al., 1999):

$$R_n = H + \lambda ET + G + \varepsilon, \qquad (1)$$

where R_n is the net radiation (positive flux towards the surface), H and λET are the turbulent sensible and latent heat fluxes (positive away from the surface), respectively, G is the soil heat flux (positive flux into the soil) at the surface, and ε is residual energy involved in other processes, such as canopy heat storage, photosynthesis, respiration and advection. All terms have units of W m^{-2}.

R_n consists of both incoming (↓) and outgoing (↑) shortwave radiation (K) and longwave radiation (L):

Accepted for publication in *Journal of Applied Meteorology and Climatology*. DOI 10.1175/JAMC-D-20-0233.1.

$$R_n = K_\downarrow + L_\downarrow - K_\uparrow - L_\uparrow. \quad (2)$$

H and λET are calculated from the EC observations with (Kaimal and Finnigan, 1994; Burba et al., 2013; Zhang et al., 2016):

$$H = \rho c_p \overline{w'T'}, \quad (3)$$

$$\lambda ET = \lambda \frac{M_w/M_a}{\bar{P}} \bar{\rho} \; \overline{w'e'}, \quad (4)$$

where w', T' and e' are the turbulent fluctuations from the mean of the vertical wind velocity (m s^{-1}), air temperature (K), and water vapor pressure (hPa), respectively, ρ is the air density (kg m^{-3}), c_p is the specific heat capacity of air at constant pressure (J kg^{-1} K^{-1}), λ is the latent heat of vaporization (J kg^{-1}), M_w and M_a are the water and air molar mass (g mol^{-1}), P is the air pressure (hPa) and ET is the crop evapotranspiration (mm s^{-1}). The three-dimensional sonic anemometer original records (10 Hz) were processed prior to analysis using the methods in Section 2b.

Because of the lack of water temperature measurements, the temperature variation at a depth of 0.05 m was used to compute the water heat storage (Timm et al., 2014). Thus, G was estimated through the sum of G at a depth (of the heat flux plate) of 0.05 m ($G_{0.05}$) and the soil and water heat storage (G_w):

$$G = G_{0.05} + C_s \Delta z_s \left(\frac{\Delta T_{0.05}}{\Delta t}\right) + G_w, \quad (5)$$

$$G_w = C_w \Delta z_w \left(\frac{\Delta T_{0.05}}{\Delta t}\right), \quad (6)$$

where C_s is the volumetric heat capacity of the soil (J m^{-3} K^{-1}) and C_w is the volumetric heat capacity of water (4.186 × 10^6 J m^{-3} K^{-1}). $\Delta T_{0.05}$ is the change in soil temperature at the depth of 0.05 m during the 30 min measurement period (Δt). Δz_s is

Accepted for publication in *Journal of Applied Meteorology and Climatology*. DOI 10.1175/JAMC-D-20-0233.1.

the thickness of the soil layer to the surface (i.e., 0.05 m), and Δz_w is the depth of the water layer (i.e., 0.15 m at the rice vegetative stages and 0.05 m at the rice reproductive stages; Section 2a). G_w appears during the soil flooding (i.e., rice vegetative and reproductive stages in Figure 1).

The $\mathcal{E}$ term (or size of the lack of energy balance closure (EBC)) was assessed using two methods. First, across multiple 30 min periods, the ordinary linear regression slope between the sum of turbulent heat fluxes ($H + \lambda ET$) and the available energy ($R_n - G$) was determined. Here, the slope was forced through 0. Second, the EBC ratio (hereafter EBR) was calculated from the 30 min data for periods of observation (Cui and Chui, 2019):

$$\mathrm{EBR} = \frac{H+\lambda ET}{R_n-G} \;. \quad (7)$$

d. Stability and footprint analysis

The Obukhov length L can be derived from (Stull, 1988):

$$L = \frac{-{u_*}^3}{k(g/\theta)\overline{w'\theta'}}, \quad (8)$$

where u_* is friction velocity (m s^{-1}), θ is the potential temperature, k (= 0.4) is the von Kármán constant (Paulson, 1970), and g (= 9.8 m s^{-2}) is the acceleration of gravity.

The dimensionless atmospheric stability parameter (ζ) was calculated according to Stull (1988), as follows:

$$\zeta = z'/L, \quad (9)$$

Accepted for publication in *Journal of Applied Meteorology and Climatology*. DOI 10.1175/JAMC-D-20-0233.1.

where $z' = z_m - z_d$, in which z_m is the observation height of the sonic anemometer (10 m) and z_d is the zero-plane displacement height estimated using the Martano (2000) approach (details in Text S1). We used three ζ classes: (1) stable ($\zeta \geq 0.01$), (2) neutral ($|\zeta|<0.01$), and (3) unstable ($\zeta \leq -0.01$).

The Kljun et al. (2015) two-dimensional flux footprint tool (http://geography.swansea.ac.uk/nkljun/ffp/www/, last access: 17 July 2018) is applicable to conditions when $u_* > 0.1$ m s^{-1} and $\zeta \geq -15.5$. It requires z_m, aerodynamic roughness length (z_0; method of Martano (2000) – see Text S1), z_d (Martano, 2000), 30 min mean wind velocity ($\overline{u}\ (z_m)$, m s^{-1}), crosswind variance (σ_v, m s^{-1}), L and u_*. As shown in Figure S1, z_0 changed with the growth of the rice and wheat, with the monthly median of z_0 varying between 0.01 and 0.08.

In the three-year study period, the source area that contributed 90% to the fluxes was smallest (average fetch length: 865 m) under unstable conditions (42% of all measurements) and largest (average fetch length: 1005 m) under stable conditions (46% of all measurements) (Table 2). The footprint extent for all measurements was largest towards the east. This was the dominant wind direction (Figure 2).

Based on these results, we estimated the land-cover fractions retrieved from a Google Earth image on 6 February 2016. The compositions in the 70–90% footprints of the 10 m tower were separated into two categories: impervious (including both buildings and roads) and cropland (Table 2). From the analysis of the 30 min EC 90% probable footprint (Kljun et al., 2015; Section 2d) climatology during the three-year

Accepted for publication in *Journal of Applied Meteorology and Climatology*. DOI 10.1175/JAMC-D-20-0233.1.

study period, the area observed included cropland (88–96%) plus a small proportion of impervious surfaces (6–12%) (Table 2), indicating that the measured fluxes were primarily contributed by the cropland.

3. Results

a. Climatological conditions

With the subtropical monsoon climate, all the meteorological variables have a marked seasonal cycle (Figure 3). The mean 10 m wind speed for the three cropping years (2014–15 to 2016–17) was slightly higher in the winter wheat season (2.6 m s^{-1}) than the summer rice season (2.4 m s^{-1}) (Figure 3a). The annual mean air temperature (at 10 m agl) for the three consecutive cropping years was 11.8°C, 13.1°C and 14.3°C, respectively (Figure 3b), which were lower than the 30-year-average annual mean air temperature (Section 2a) in the study area. It was much higher in the growing season of summer rice (22.1°C) than that of winter wheat (11.8°C).

Similar seasonal patterns were evident in the vapor pressure deficit (*VPD*) (Figure 3c). The average *VPD* of the site was high in summer (5 hPa) and low in winter (3 hPa). Surface-level air pressure exhibited an inverse relation with air temperature (Figures 3b, d). The annual precipitation for the 2015–16 and 2016–17 crop years were similar (1587 and 1640 mm, respectively) and larger than for 2014–15 (1226 mm) (Figure 3e). The latter was more comparable to the 30-year mean (Section 2a). Most precipitation

Accepted for publication in *Journal of Applied Meteorology and Climatology*. DOI 10.1175/JAMC-D-20-0233.1.

occurred from June to October, with the maximum daily precipitation of 321 mm on 10th August 2015 caused by Super Typhoon Soudelor.

b. Radiation and other surface energy fluxes

All four components of the radiation budget (Eq. 2) and surface albedo were observed in this study (Figure 4). As expected, seasonal variations in solar radiation received at the surface depended mainly on solar altitude and cloud conditions. At this site, the monthly median $K_{\downarrow}$ ($K_{\uparrow}$) ranged from 151 (20) W m^{-2} in October to 825 (126) W m^{-2} in May. The seasonal variations of $L_{\downarrow}$ and $L_{\uparrow}$ were similar, with higher values in the summer rice growing season than in the winter wheat growing period. The July daily $L_{\downarrow}$ peaks were 477, 470 and 485 W m^{-2} across the three consecutive years, whereas for $L_{\uparrow}$ these were 540, 537 and 547 W m^{-2}.

Surface albedo varied with surface conditions, including leaf growth. The seasonal mean albedo was larger for winter wheat (2014–15: 0.19; 2015–16: 0.20; and 2016–17: 0.18) than summer rice (0.11, 0.10 and 0.09, respectively). Key influences were the flooded early rice period (June to July, Figure 1c) and the winter (December to February) extensive bare soil period (Figure 1f). The average bare soil albedo (0.15) was greater than that for water (0.12). Additionally, the largest daily values occurred with winter snow. The maximum observed daily mean was 0.53 (29 January 2015).

There were considerable differences in surface radiation balance between years. The annual mean albedo in 2016–17 was smaller than in the two earlier years (Table 3), with less shortwave radiation reflected into the atmosphere. The slightly smaller soil temperatures in 2014–15 were associated with the smaller $L_{\uparrow}$ (Table 3). Together, these factors contributed to the greater R_n in 2016–17 (Table 3).

Accepted for publication in *Journal of Applied Meteorology and Climatology*. DOI 10.1175/JAMC-D-20-0233.1.

All of the energy balance fluxes varied seasonally (Figure 5). Over the three years (1 June 2014 to 31 May 2017), the monthly medians varied from 110 to 592 W m^{-2} for R_n, 62 to 361 W m^{-2} for λET, 5 to 101 W m^{-2} for H, and −3 to 65 W m^{-2} for G. In seasonal average terms, the rice paddies had 52% more λET than the wheat field. The wheat, on the other hand, had significantly more (73%) H than the rice paddies. The λE and H seasonal variations observed for the rice–wheat rotation were similar to other ecosystems (Bi et al., 2007; Wu et al., 2007; Gao et al., 2009). The response to phenological changes was evident, such as to the emergence of new leaves in February (June) over the wheat field (rice paddy) and the rapid senescence from May (September). Other seasonal fluctuations in H and λET were related to agricultural activities (e.g., choice of crop type, crop rotation, harvest time, and intermittent irrigation; Section 2a). H also increased as the crop got drier before the harvest (late May to early June).

c. Evapotranspiration

Seasonal variations in the 8-day leaf area index (*LAI*) and daily total *ET* for the 2014–17 cropping periods over the rice–wheat rotation systems are shown in Figure 6. Mean *LAI* was slightly higher in the growing season of summer rice (1.3) than that of winter wheat (1.0). For rice, peak *LAI* of 3.5, 5.4 and 4.2 m^2 m^{-2} were observed during the reproductive stages (late August or early September) of 2014, 2015 and 2016,

Accepted for publication in *Journal of Applied Meteorology and Climatology*. DOI 10.1175/JAMC-D-20-0233.1.

respectively. Peak *LAI* values for wheat were 2.7, 2.6, and 2.2 m^2 m^{-2} in April 2015, 2016 and 2017, respectively.

The daily *ET* of wheat increased consistently with a concurrent gradual increase in *LAI* (Figure 6a). As the wheat reached its peak *LAI* during the reproductive growth stages (around April), *ET* also reached its peak values. After the reproductive stages, wheat's *LAI* started to decrease due to the canopy senescence. For rice, a high *ET* occurred during the vegetative stages mainly due to the higher evaporation of flooded water rather than transpiration since the plants were still small (*LAI*<1, Alberto et al., 2011). The average daily *ET* for rice and wheat growing seasons were 3.6 mm d^{-1} and 2.4 mm d^{-1}, indicating a higher water consumption for rice than for wheat. Generally, rice paddies had higher *ET* than wheat fields, probably due to the absence of ponded water (Figure 1c and 1d) and lower *LAI* of wheat (Figure 6a) (Alberto et al., 2011).

d. Energy partitioning

The proportion of R_n used in H, λET and G (H/R_n, $\lambda ET/R_n$, and G/R_n) varied seasonally with land surface conditions (Figure 7). Generally, the middle of the day (10:00–16:00 LST) H/R_n and Bowen ratio ($\beta = H/\lambda ET$) had an inverse trend to $\lambda ET/R_n$, while EBR (Eq. 7) had a similar trend to $\lambda ET/R_n$. The EBR was larger during the day (0.67 to 0.99) than during the middle of the night (22:00–04:00 LST, −0.14 to 0.57). Consistent with Wilson et al. (2002) and Majozi et al. (2017), the nocturnal EBRs were less than the midday-period EBRs as the calm midnight period suppressed turbulence

Accepted for publication in *Journal of Applied Meteorology and Climatology*. DOI 10.1175/JAMC-D-20-0233.1.

that was essential for the creation of eddies. Annually, the median midday λET was the largest consumer of the R_n (52%, 60% and 62% of R_n in 2014–15, 2015–16 and 2016–17, respectively), while the annual midday $\lambda ET/R_n$ was largest in 2016–17 given the larger precipitation in 2016–17 (Section 3a). The median midday H/R_n (G/R_n) was 18% (15%), 13% (9%) and 15% (6%) in 2014–15, 2015–16 and 2016–17, respectively. In the midday period, rice paddies had a higher (70%) $\lambda ET/R_n$ than the wheat (53%), because of the extensive presence of water (Figure 1c). Thus, wheat had a larger median midday β in the three years (0.42, 0.35, 0.42) than rice (0.19, 0.13, 0.10).

G during the mid-night period (20:00–04:00 LST) was the largest component of energy. The median G/R_n values varied between 97% (2014–15), 83% (2015–16), and 65% (2016–17). The radiative surface cooling was maintained by the G (approximately −20 W m^{-2}) conducting heat back towards the surface. As expected, the median midday β was positive (0.04 to 0.66). However, β was negative in the midnight period (−2.18 to −0.08) as small positive λET (10 W m^{-2}) often occurred, with small negative H (−10 W m^{-2}) values maintained by radiative cooling, conduction, and release of heat with condensation.

e. Energy balance closure

Here, we consider the effect of crop type and different growth stages on the EBC. The regression slope (forced through 0) was less than 1 for all growth stages (0.59 to 0.95), with a coefficient of determination (R^2) between 0.60 and 0.88 (Table 4). This

Accepted for publication in *Journal of Applied Meteorology and Climatology*. DOI 10.1175/JAMC-D-20-0233.1.

was consistent with the slope reported in Wilson et al. (2002), ranging between 0.53 and 0.99 and obtained from the analysis of 22 FLUXNET sites. The wheat EBC improved across the three growth stages (vegetative < reproductive < ripening; Table 4). Better EBC occurred at the vegetative stages for rice after considering the G_w (Table 4). When G_w was included in the energy balance closure, the slope improved from 0.75 to 0.91 and 0.76 to 0.88 at the rice vegetative stages in 2015–16 and 2016–17, respectively.

4. Discussion

a. Comparisons of ET with other sites

To eliminate the uncertainties caused by experimental methods, we only collected *ET* data from studies based on EC measurements. As can be seen in Table 5, the cumulative *ET* for the whole rice growing season was 473 mm, which was comparable to that reported in the Taihu Lake region of China (Liu et al., 2018), and lower than that reported in the Philippines (Alberto et al., 2011; Alberto et al., 2014), but greater than the water consumption reported in Japan (Ikawa et al., 2017) and Brazil (Timm et al., 2014). The differences in the total seasonal *ET* observed from the above studies may be due to the differences in agricultural production activities (such as crop type, growth periods and irrigation), physiological characteristics (e.g., *LAI*) and meteorological conditions (Liu et al., 2018; Qiu et al., 2019). For example, the cumulative *ET* was highest at the Laguna site (499 mm, Table 5) in the Philippines, which was located in

Accepted for publication in *Journal of Applied Meteorology and Climatology*. DOI 10.1175/JAMC-D-20-0233.1.

the tropical region with high air temperature (about 27 °C) and high VPD (about 0.8 kPa). Furthermore, rice paddy (473 mm) had a higher mean growing season *ET* rate than that for the wheat field (387 mm) at our site (Table 5). For winter wheat, the cumulative *ET* at our site was lower than the values reported in northern China (401–417 mm, Lei and Yang, 2010; Zhang et al., 2013). The growth period of winter wheat in our area was shorter than that in northern China, which had an inhibited effect on crop growth and canopy coverage (Qiu et al., 2019).

The average daily *ET* rate for rice over the growing season was 3.6 mm d^{-1}, which was close to the values in the similar temperate climate zone (e.g., China, Japan and Brazil), and higher than that in boreal zone (2.8 mm d^{-1}), but lower than that in tropical zone (4–4.2 mm d^{-1}, Table 5). Also, the daily *ET* rate occurred in our wheat fields was 2.4 mm d^{-1}, which was higher than the arid regions in northern China. Generally, the daily *ET* rate gradually decreased from tropical to temperate and boreal zones, which was comparable to the findings reported in Kang and Cho (2021).

b. The effect of crop type and growth stages on EBC

Generally, EBC had a marked seasonal variation in the rice paddies and wheat fields. For wheat, EBC improved as the growth stages progressed. During the ripening stages, wheat leaves gradually turned yellow (*LAI* <2, Figure 6) and photosynthetic rates became weaker. The energy fluxes for photosynthesis showed a lower contribution to EBC (within 2%) during the ripening phase of winter wheat (Eshonkulov et al.,

Accepted for publication in *Journal of Applied Meteorology and Climatology*. DOI 10.1175/JAMC-D-20-0233.1.

2019). Furthermore, in the maturity phase of winter wheat, canopy heat storage (1% to available energy, Eshonkulov et al., 2019) also distinctly decreased due to lower plant water content (Meyers and Hollinger, 2004). Our research demonstrated that u_* played a key role in improving EBC at the ripening stages. The canopy height of wheat was higher and wheat fields became more homogeneous during later crop development stages (Figure 1f-h, Stoy et al., 2013). Higher mean u_* (> 0.28 m s^{-1}) occurred during the wheat ripening stages, resulting in a stronger development of turbulence over wheat fields (Barr et al., 2006; Tanaka et al., 2008; Franssen et al., 2010). For rice, better EBC occurred at the vegetative stages. According to Timm et al. (2014), we also estimated the storage energy in water using the temperature variation at a depth of 0.05 m below the ground surface. The EBC improved by 19% during this period by adding G_w. This result indicated that G_w makes a non-negligible contribution to the surface energy balance (Hossen et al., 2012). Ikawa et al. (2017), also in a rice paddy study, reported that EBC improved by 12% after accounting for the 3 cm depth water storage. As expected, the effect was greater at our site than the values reported in Ikawa et al. (2017) because the 15 cm of standing water at our site was deeper.

Because the EC flux was measured at a relatively high height (10 m, Figure 1), there might also have been a possibility that the effect of large-scale transports differentiated the energy balance between summer and winter. In the presence of such large-scale organized structures, single-tower measurements must be biased, because the associated vertical energy transport is inherently not captured (Etling and Brown,

Accepted for publication in *Journal of Applied Meteorology and Climatology*. DOI 10.1175/JAMC-D-20-0233.1.

1993; Mauder et al., 2020). Thus, multi-tower experiments and scale-crossing, spatially resolving lidar and airborne measurements with high-resolution large-eddy simulations will be considered in our future work.

5. Summary and conclusions

From the analysis of the seasonal and interannual variability of meteorological conditions including radiation and turbulent fluxes, *ET*, energy partitioning and EBC over a rice–wheat rotation system in East China (1 June 2014 to 31 May 2017) were studied. The key findings are as follows:

As expected, given wheat was grown in the winter, the summer rice growing season was warmer but also more humid and received more precipitation. For our study site, rice paddies (473 mm) had higher *ET* than the wheat fields (387 mm), probably due to the absence of ponded water and lower *LAI* of wheat. Across the whole rice-wheat rotation, the average daily *ET* rate in the rice paddies and wheat fields was 3.6 mm d^{-1} and 2.4 mm d^{-1}, respectively. Considering the seasonal distribution of precipitation and agricultural production activities (such as crop type and irrigation), the rice paddies had 52% more λET than the wheat fields given the extensive water availability. Consequently, the wheat fields had a significantly higher Bowen ratio (0.4) than the rice paddies (0.14). During the observation period, the annual precipitation fluctuated between 1226 mm (2014–15) and 1640 mm (2016–17), causing large annual variations in $\lambda ET/R_n$ (annual midday (10:00–16:00) values between 52% (2014–15) and 62% (2016–17)). On an annual basis, for the entire rice–wheat rotation, the

Accepted for publication in *Journal of Applied Meteorology and Climatology*. DOI 10.1175/JAMC-D-20-0233.1.

dominant ratio for the midday period was $\lambda ET/R_n$, whereas nocturnally (22:00–04:00 LST) it was G/R_n. EBC was greatest at the rice vegetative growth stages after considering the water heat storage, whereas for wheat it was greatest at the ripening stages. Overall, EBC was greater for rice (0.85) than for wheat (0.76).

These new data on intra- and interannual variations of fluxes provide a new understanding of the differences between rice and wheat growing seasons. These data will be beneficial for improving models to simulate surface energy exchanges for the extensive area of rice–wheat agroecosystems in Asian countries.

Acknowledgments

This work was supported by the National Natural Science Foundation of China (Nos. 41875013 and 41711530223), Royal Society–Newton Mobility funding (IE161543), and the Newton Fund/Met Office CSSP-China (SG). The authors declare no conflicts of interest. We are very grateful to the anonymous reviewers for their careful review and valuable comments, which led to a substantial improvement of the manuscript.

Accepted for publication in *Journal of Applied Meteorology and Climatology*. DOI 10.1175/JAMC-D-20-0233.1.

REFERENCES

Alberto, Ma Carmelita R, Wassmann Reiner, Hirano Takashi, Miyata Akira, Kumar Arvind, et al. (2009). CO_2/heat fluxes in rice fields: Comparative assessment of flooded and non-flooded fields in the Philippines. *Agricultural and Forest Meteorology*, *149*(10), 1737-1750. https://doi.org/10.1016/j.agrformet.2009.06.003

Alberto, R, M. C., Wassmann, R., Hirano, T., Miyata, A., Hatano, R., et al. (2011). Comparisons of energy balance and evapotranspiration between flooded and aerobic rice fields in the Philippines, *Agricultural Water Management*, *98*(9), 1417-1430.

Alberto, M. C. R., Quilty, J. R., Buresh, R. J., Wassmann, R., Haidar, S., Correa, T. Q., & Sandro, J. M. (2014). Actual evapotranspiration and dual crop coefficients for dry-seeded rice and hybrid maize grown with overhead sprinkler irrigation. *Agricultural Water Management*, *136*, 1-12. https://doi.org/10.1016/j.agwat.2014.01.005

Baldocchi, D. D. (2003). Assessing the eddy covariance technique for evaluating carbon dioxide exchange rates of ecosystems: past, present and future. *Global Change Biology*, *9*(4), 479-492. https://doi.org/10.1046/j.1365-2486.2003.00629.x

Accepted for publication in *Journal of Applied Meteorology and Climatology*. DOI 10.1175/JAMC-D-20-0233.1.

Barr, A. G., Morgenstern, K., Black, T. A., McCaughey, J. H., & Nesic, Z. (2006). Surface energy balance closure by the eddy-covariance method above three boreal forest stands and implications for the measurement of the CO2 flux. *Agricultural and Forest Meteorology*, *140*(1), 322-337. https://doi.org/10.1016/j.agrformet.2006.08.007

Bi, X., Gao, Z., Deng, X., Wu, D., Liang, J., Zhang, H., et al. (2007). Seasonal and diurnal variations in moisture, heat, and CO_2 fluxes over grassland in the tropical monsoon region of southern China. *Journal of Geophysical Research-Atmospheres*, *112*(D10), 106-120. https://doi.org/10.1029/2006jd007889

Burba, G., G., VERMA, S., B., & KIM (1999). Surface energy fluxes of Phragmites australis in a prairie wetland. *Agricultural & Forest Meteorology*, *94*(1), 31-51. https://doi.org/10.1016/S0168-1923(99)00007-6

Burba, G., 2013. Eddy Covariance Method for Scientific, Industrial, Agricultural and Regulatory Applications: A Field Book on Measuring Ecosystem Gas Exchange and Areal Emission Rates. LI-COR Biosciences, Lincoln, USA, Hard- and Softbound, 331 pp. ISBN: 978-0-61576827-4

Cui, W., & Chui, T. F. M. (2019). Temporal and spatial variations of energy balance closure across FLUXNET research sites. *Agricultural and Forest Meteorology*, *271*, 12-21. https://doi.org/10.1016/j.agrformet.2019.02.026

Ding, R., Kang, S., Li, F., Zhang, Y., & Tong, L. (2013). Evapotranspiration measurement and estimation using modified Priestley–Taylor model in an

Accepted for publication in *Journal of Applied Meteorology and Climatology*. DOI 10.1175/JAMC-D-20-0233.1.

irrigated maize field with mulching. *Agricultural and Forest Meteorology*, *168*, 140-148. https://doi.org/10.1016/j.agrformet.2012.08.003

Eshonkulov, R., Poyda, A., Ingwersen, J., Pulatov, A., & Streck, T. (2019). Improving the energy balance closure over a winter wheat field by accounting for minor storage terms. *Agricultural and Forest Meteorology*, 264, 283-296. https://doi.org/10.1016/j.agrformet.2018.10.012

Etling, D., & Brown, R. J. B.-L. M. (1993). Roll vortices in the planetary boundary layer: A review, *65*(3), 215-248.

Franssen, H. H., Stöckli, R., Lehner, I., Rotenberg, E., & Seneviratne, S. I. (2010). Energy balance closure of eddy-covariance data: A multisite analysis for European FLUXNET stations. *Agricultural and Forest Meteorology*, *150*(12), 1553-1567. https://doi.org/10.1016/j.agrformet.2010.08.005

Gao, Z., Bian, L., & Zhou, X. (2003). Measurements of turbulent transfer in the near-surface layer over a rice paddy in China. *Journal of Geophysical Research*, *108*(D13), 4387. https://doi.org/10.1029/2002JD002779

Gao, Z., Lenschow, D., He, Z., & Zhou, M. (2009). Seasonal and diurnal variations in moisture, heat and CO_2 fluxes over a typical steppe prairie in Inner Mongolia, China. *Hydrology and Earth System Sciences*, *13*(7), 987-998. https://doi.org/10.5194/hess-13-987-2009

Garratt, J. R. (1992). *The atmospheric boundary layer.*

Accepted for publication in *Journal of Applied Meteorology and Climatology*. DOI 10.1175/JAMC-D-20-0233.1.

Ge, H. X., Zhang, H. S., Zhang, H., Cai, X. H., Song, Y., & Kang, L. (2018). The characteristics of methane flux from an irrigated rice farm in East China measured using the eddy covariance method. *Agricultural and Forest Meteorology*, *249*, 228-238. https://doi.org/10.1016/j.agrformet.2017.11.010

Hossen, M. S., Mano, M., Miyata, A., Baten, M. A., & Hiyama, T. (2012). Surface energy partitioning and evapotranspiration over a double-cropping paddy field in Bangladesh. *Hydrological Processes*, *26*(9), 1311-1320. 10.1002/hyp.8232

Ikawa, H., Ono, K., Mano, M., Kobayashi, K., Takimoto, T., Kuwagata, T., & Miyata, A. (2017). Evapotranspiration in a rice paddy field over 13 crop years. *Journal of Agricultural Meteorology*, *73*(3), 109-118. 10.2480/agrmet.D-16-00011

Jia, X., Zha, T. S., Gong, J. N., Wu, B., Zhang, Y. Q., Qin, S. G., et al. (2016). Energy partitioning over a semi-arid shrubland in northern China, *30*(6), 972-985. https://doi.org/10.1002/hyp.10685

Jin, Z. Q., Shah, T. R., Zhang, L., Liu, H. Y., Peng, S. B., & Nie, L. X. (2020). Effect of straw returning on soil organic carbon in rice-wheat rotation system: A review. *Food and Energy Security*, 13. https://doi.org/10.1002/fes3.200

Kaimal, J. C., & Finnigan, J. J. (1994). *Atmospheric Boundary Layer Flows: Their Structure and Measurement.* Oxford University Press.

Kang, M., & Cho, S. (2021). Progress in water and energy flux studies in Asia: A review focused on eddy covariance measurements. *Journal of Agricultural Meteorology*, *77*(1), 2-23.

Accepted for publication in *Journal of Applied Meteorology and Climatology*. DOI 10.1175/JAMC-D-20-0233.1.

Kljun, N., Calanca, P., Rotach, M. W., & Schmid, H. P. (2015). A simple two-dimensional parameterisation for Flux Footprint Prediction (FFP). *Geosci. Model Dev.*, *8*(11), 3695-3713. 10.5194/gmd-8-3695-2015

Kumari, M., Chakraborty, D., Gathala, M. K., Pathak, H., Dwivedi, B. S., Tomar, R. K., et al. (2011). Soil Aggregation and Associated Organic Carbon Fractions as Affected by Tillage in a Rice–Wheat Rotation in North India. *Soil Science Society of America Journal*, *75*(2), 560-567. https://doi.org/10.2136/sssaj2010.0185

Lan, T., Li, M., Han, Y., Deng, O., Tang, X., Luo, L., et al. (2020). How are annual CH4, N2O, and NO emissions from rice–wheat system affected by nitrogen fertilizer rate and type? *Applied Soil Ecology*, *150*, 103469. https://doi.org/10.1016/j.apsoil.2019.103469

Lee, X., Massman, W., & Law, B. (2004). *Handbook of micrometeorology: a guide for surface flux measurement and analysis.* Springer Science & Business Media.

Lei, H., & Yang, D. (2010). Interannual and seasonal variability in evapotranspiration and energy partitioning over an irrigated cropland in the North China Plain. *Agricultural & Forest Meteorology*, *150*(4), 581-589. https://doi.org/10.1016/j.agrformet.2010.01.022

Li, X., Gao, Z., Li, Y., & Tong, B. (2017). Comparison of sensible heat fluxes measured by a large aperture scintillometer and eddy covariance system over a

Accepted for publication in *Journal of Applied Meteorology and Climatology*. DOI 10.1175/JAMC-D-20-0233.1.

heterogeneous farmland in east China. *Atmosphere*, *8*(6), 101. https://doi.org/10.3390/atmos8060101

Liu, B., Cui, Y., Luo, Y., Shi, Y., Liu, M., & Liu, F. (2019). Energy partitioning and evapotranspiration over a rotated paddy field in Southern China. *Agricultural and Forest Meteorology*, *276-277*, 107626.

Liu, X. Y., Xu, J. Z., Yang, S. H., & Zhang, J. G. (2018). Rice evapotranspiration at the field and canopy scales under water-saving irrigation. *Meteorology and Atmospheric Physics*, *130*(2), 227-240. 10.1007/s00703-017-0507-z

Ma, N., Zhang, Y., Guo, Y., Gao, H., Zhang, H., & Wang, Y. J. J. o. H. (2015). Environmental and biophysical controls on the evapotranspiration over the highest alpine steppe, *529*, 980-992.

Majozi, N. P., Mannaerts, C. M., Ramoelo, A., Mathieu, R., Nickless, A., & Verhoef, W. (2017). Analysing surface energy balance closure and partitioning over a semi-arid savanna FLUXNET site in Skukuza, Kruger National Park, South Africa. *Hydrology and Earth System Sciences*, *21*(7), 3401-3415. https://doi.org/10.5194/hess-21-3401-2017

Martano, P. (2000). Estimation of Surface Roughness Length and Displacement Height from Single-Level Sonic Anemometer Data. *Journal of Applied Meteorology Climatology*, *39*(5), 708-715. 10.1175/1520-0450(2000)039<0708:Eosrla>2.0.Co;2

Masseroni, D., Facchi, A., Romani, M., Chiaradia, E. A., Gharsallah, O., & Gandolfi,

C. (2015). Surface energy flux measurements in a flooded and an aerobic rice field using a single eddy-covariance system. *Paddy and Water Environment*, *13*(4), 405-424. 10.1007/s10333-014-0460-0

Mauder, M., Foken, T., & Cuxart, J. (2020). Surface‐ Energy‐ Balance Closure over Land: A Review. *Boundary-Layer Meteorol.* https://doi.org/10./s10546-020-00529-6

Meyers, T. P., & Hollinger, S. E. (2004). An assessment of storage terms in the surface energy balance of maize and soybean. *Agricultural and Forest Meteorology*, *125*(1), 105-115. https://doi.org/10.1016/j.agrformet.2004.03.001

Moncrieff, J., Clement, R., Finnigan, J., & Meyers, T. (2004). *Averaging, Detrending, and Filtering of Eddy Covariance Time Series.* doi:https://doi.org/10.1007/1-4020-2265-4_2.

Oncley, S. P., Foken, T., Vogt, R., Kohsiek, W., Debruin, H. A. R., Bernhofer, C., et al. (2007). The Energy Balance Experiment EBEX-2000. Part I: overview and energy balance. *Boundary-Layer Meteorology*, *123*(1), 1-28. https://doi.org/10.1007/s10546-007-9161-1

Paulson, C. A. (1970). The mathematical representation of wind speed and temperature profiles in the unstable atmospheric surface layer. *Journal of Applied Meteorology*, *9*(6), 857-861. https://doi.org/10.1175/1520-0450(1970)009<0857:TMROWS>2.0.CO;2

Accepted for publication in *Journal of Applied Meteorology and Climatology*. DOI 10.1175/JAMC-D-20-0233.1.

Qiu, R., Liu, C., Cui, N., Wu, Y., Wang, Z., & Li, G. (2019). Evapotranspiration estimation using a modified Priestley-Taylor model in a rice-wheat rotation system. *Agricultural Water Management*, *224*, 105755. https://doi.org/10.1016/j.agwat.2019.105755

Schmidt, M., Reichenau, T. G., Fiener, P., & Schneider, K. (2012). The carbon budget of a winter wheat field: An eddy covariance analysis of seasonal and inter-annual variability. *Agricultural and Forest Meteorology*, *165*, 114-126. https://doi.org/10.1016/j.agrformet.2012.05.012

Stoy, P. C., Mauder, M., Foken, T., Marcolla, B., Boegh, E., Ibrom, A., et al. (2013). A data-driven analysis of energy balance closure across FLUXNET research sites: The role of landscape scale heterogeneity. *Agricultural and Forest Meteorology*, *171-172*, 137-152. 10.1016/j.agrformet.2012.11.004

Stull, R. B. (1988). An introduction to boundary layer meteorology. *Atmospheric Sciences Library*, *8*(8), 89.

Tanaka, H., Hiyama, T., Kobayashi, N., Yabuki, H., Ishii, Y., Desyatkin, R. V., et al. (2008). Energy balance and its closure over a young larch forest in eastern Siberia. *Agricultural and Forest Meteorology*, *148*(12), 1954-1967. https://doi.org/10.1016/j.agrformet.2008.05.006

Timm, A. U., Roberti, D. R., Streck, N. A., Gustavo G. de Goncalves, L., Acevedo, O. C., Moraes, O. L. L., et al. (2014). Energy Partitioning and Evapotranspiration over a Rice Paddy in Southern Brazil. *Journal of*

Accepted for publication in *Journal of Applied Meteorology and Climatology*. DOI 10.1175/JAMC-D-20-0233.1.

Hydrometeorology, 15(5), 1975-1988. https://doi.org/10.1175/JHM-D-13-0156.1

Timsina, J., & Connor, D. J. (2001). Productivity and management of rice–wheat cropping systems: issues and challenges. *Field Crops Research*, *69*(2), 93-132.

Tsai, J. L., Tsuang, B. J., Lu, P. S., Yao, M. H., & Shen, Y. (2007). Surface Energy Components and Land Characteristics of a Rice Paddy. *Journal of Applied Meteorology & Climatology, 46*(11), 1879-1900. https://doi.org/10.1016/S0378-4290(00)00143-X

Webb, E. K., Pearman, G. I., & Leuning, R. (1980). Correction of flux measurements for density effects due to heat and water vapour transfer. *Quarterly Journal of the Royal Meteorological Society*, *106*(447), 85-100. https://doi.org/10.1002/qj.49710644707

Wilson, K., Goldstein, A., Falge, E., Aubinet, M., Baldocchi, D., Berbigier, P., et al. (2002). Energy balance closure at FLUXNET sites. *Agricultural and Forest Meteorology, 113*(1-4), 223-243. https://doi.org/10.1016/S0168-1923(02)00109-0

Wu, J., Guan, D., Han, S., Shi, T., Jin, C., Pei, T., & Yu, G. (2007). Energy budget above a temperate mixed forest in northeastern China. *Hydrological Processes: An International Journal*, *21*(18), 2425-2434. https://doi.org/10.1002/hyp.6395

Accepted for publication in *Journal of Applied Meteorology and Climatology*. DOI 10.1175/JAMC-D-20-0233.1.

Yan, H., Zhang, C., Oue, H., Wang, G., He, B. J. T., & climatology, a. (2015). Study of evapotranspiration and evaporation beneath the canopy in a buckwheat field, *122*(3), 721-728.

Yang, F., Zhang, Q., Hunt, J. E., Zhou, J., Sha, S., Li, Y., et al. (2019). Biophysical regulation of evapotranspiration in semiarid croplands. *Journal of Soil and Water Conservation*, *74*(3), 309-318. 10.2489/jswc.74.3.309

You, Q., Xian, X., Fei, P., Dong, S., & Gao, Y. (2017). Surface water and heat exchange comparison between alpine meadow and bare land in a permafrost region of the Tibetan Plateau. *Agricultural & Forest Meteorology*, *232*(Complete), 48-65. https://doi.org/10.1016/j.agrformet.2016.08.004

Zhang, B., Liu, Y., Xu, D., Zhao, N., Lei, B., Rosa, R. D., et al. (2013). The dual crop coefficient approach to estimate and partitioning evapotranspiration of the winter wheat–summer maize crop sequence in North China Plain. *Irrigation Science*, *31*(6), 1303-1316. 10.1007/s00271-013-0405-1

Zhang, B., Xu, D., Liu, Y., Li, F., Cai, J., & Du, L. (2016). Multi-scale evapotranspiration of summer maize and the controlling meteorological factors in north China. *Agricultural and Forest Meteorology*, *216*, 1-12. https://doi.org/10.1016/j.agrformet.2015.09.015

Zhao, X., Huang, Y., Jia, Z., Liu, H., Song, T., Wang, Y., et al. (2008). Effects of the conversion of marshland to cropland on water and energy exchanges in

Accepted for publication in *Journal of Applied Meteorology and Climatology*. DOI 10.1175/JAMC-D-20-0233.1.

northeastern China. *Journal of Hydrology*, *355*(1), 181-191. https://doi.org/10.1016/j.jhydrol.2008.03.019

Zhao, X., Xie, Y. x., Xiong, Z. q., Yan, X. y., Xing, G. x., & Zhu, Z. l. (2009). Nitrogen fate and environmental consequence in paddy soil under rice-wheat rotation in the Taihu lake region, China. *Plant and soil*, *319*(1-2), 225-234. https://doi.org/10.1007/s11104-008-9865-0

Accepted for publication in *Journal of Applied Meteorology and Climatology*. DOI 10.1175/JAMC-D-20-0233.1.

TABLES

Table 1: Main crop growth stages and corresponding mean canopy height (z_H) during 2014–17 (from *in situ* measurements).

Year	Crop	Growth	Vegetative	Reproductive	Ripening
2014–15	rice	duration	Jun 21–Aug 4	Aug 5–Sep 30	Oct 1–Nov 9
		z_H (m)	0.37	0.62	0.93
	wheat	duration	Dec 15–Feb 28	Mar 1–Apr 15	Apr 16–May 31
		z_H (m)	0.15	0.58	0.86
2015–16	rice	duration	Jun 20–Aug 9	Aug 10–Oct 1	Oct 2–Nov 7
		z_H (m)	0.38	0.63	0.93
	wheat	duration	Dec 10–Feb 29	Mar 1–Apr 16	Apr 17–May 25
		z_H (m)	0.15	0.60	0.87
2016–17	rice	duration	Jun 16–Aug 5	Aug 6–Sep 30	Oct 1–Nov 5
		z_H (m)	0.39	0.64	0.93
	wheat	duration	Dec 14–Feb 28	Mar 1–Apr 14	Apr 15–May 31
		z_H (m)	0.16	0.55	0.88

Accepted for publication in *Journal of Applied Meteorology and Climatology*. DOI 10.1175/JAMC-D-20-0233.1.

Table 2: Land-cover fractions within the footprints at flux contribution intervals of 70%, 80% and 90% at the 10 m flux tower site. *N* is the number of 30 min data points. Stability is defined in Section 2d.

		Unstable (*N* = 14884)	Neutral (*N* = 4329)	Stable (*N* = 16293)	Source Area (%)
Average fetch length (m)		246	259	300	70
		389	412	476	80
		865	871	1005	90
Land-cover Fraction	Impervious	0.00	0.00	0.00	70
	Crops	1.00	1.00	1.00	70
	Impervious	0.02	0.03	0.04	80
	Crops	0.98	0.97	0.96	80
	Impervious	0.06	0.09	0.12	90
	Crops	0.94	0.91	0.88	90

Accepted for publication in *Journal of Applied Meteorology and Climatology*. DOI 10.1175/JAMC-D-20-0233.1.

Table 3: Monthly median midday radiation components ($K_\downarrow$, $K_\uparrow$, $L_\downarrow$, $L_\uparrow$) in W m^{-2}, net radiation (R_n) in W m^{-2}, albedo, 0.05 m soil temperature ($T_{0.05}$) in K, and energy partitioning (H/R_n, $\lambda E/R_n$ and G/R_n) from June 2014 to May 2017.

Year	Month	Surface		$K_\downarrow$	$K_\uparrow$	$L_\downarrow$	$L_\uparrow$	R_n	Albedo	$T_{0.05}$	H/R_n	$\lambda E/R_n$	G/R_n
		Rice	Wheat										
	6	✓		524	69	422	485	392	0.135	299	0.34	–	0.26
	7	✓		549	67	447	487	429	0.126	300	0.10	–	0.30
	8	✓		455	57	435	480	345	0.120	299	0.06	–	0.08
	9	✓		396	50	418	461	306	0.125	296	–	–	0.07
	10	✓		483	77	363	444	328	0.158	292	0.12	0.62	0.17
2014–15	11		✓	263	39	353	403	169	0.149	286	0.22	0.45	0.17
	12		✓	339	52	268	354	204	0.148	278	0.24	0.36	0.13
	1		✓	233	36	300	355	143	0.138	278	0.24	0.42	0.11
	2		✓	286	44	300	364	183	0.140	279	0.23	0.43	0.13
	3		✓	398	68	331	385	267	0.166	283	0.19	0.50	0.14
	4		✓	554	100	359	413	381	0.182	289	0.11	0.70	0.20
	5		✓	529	80	392	444	390	0.144	294	0.15	0.66	0.16
	6	✓		345	46	425	463	258	0.124	296	0.20	0.58	0.13
	7	✓		462	59	440	486	363	0.121	299	0.07	0.70	0.32
	8	✓		482	69	440	485	374	0.135	299	0.03	0.76	0.10
	9	✓		454	70	421	466	333	0.154	296	0.06	0.76	0.07
	10	✓		472	81	370	440	321	0.172	292	0.11	0.71	0.07
2015–16	11		✓	162	24	365	392	112	0.151	287	0.14	0.59	0.03
	12		✓	234	31	290	362	136	0.141	280	0.17	0.47	0.05
	1		✓	245	35	292	343	152	0.144	277	0.19	0.40	0.01
	2		✓	415	59	292	369	267	0.138	279	0.21	0.39	0.09
	3		✓	473	76	324	395	330	0.154	283	0.22	0.48	0.10
	4		✓	490	80	370	425	341	0.161	289	0.08	0.69	0.08
	5		✓	380	44	391	448	287	0.119	292	0.11	0.72	0.08
	6	✓		378	42	427	466	299	0.105	297	0.16	0.59	0.14
	7	✓		544	70	452	494	425	0.123	300	0.07	0.67	0.26
	8	✓		660	94	455	503	510	0.142	302	0.05	0.73	0.06
	9	✓		439	65	417	464	319	0.144	297	0.03	0.74	0.02
	10	✓		154	20	397	422	113	0.130	293	0.05	0.85	0.00
2016–17	11		✓	206	28	338	394	135	0.133	287	0.23	0.54	0.01
	12		✓	247	37	300	367	156	0.147	282	0.23	0.49	0.01
	1		✓	211	31	300	355	133	0.147	279	0.28	0.51	0.01
	2		✓	391	66	302	362	250	0.155	279	0.28	0.46	0.03
	3		✓	575	96	301	392	384	0.166	282	0.28	0.47	0.06
	4		✓	–	–	–	–	–	–	–	–	–	–
	5		✓	567	79	401	472	426	0.136	292	0.11	0.70	0.08

Accepted for publication in *Journal of Applied Meteorology and Climatology*. DOI 10.1175/JAMC-D-20-0233.1.

Table 4: Energy balance closure at different growth stages over rice–wheat rotation during 2014–17. *N* is the number of 30 min data points. Note that there are large data gaps in the 2014 rice vegetative and reproductive growth stages due to instrument malfunction.

Crop	Year	Parameter	Vegetative	Reproductive	Ripening
Rice	2014	Slope	–	–	0.86
		R^2	–	–	0.88
		N	–	–	1079
	2015	Slope	0.91 (0.75*)	0.90 (0.86*)	0.82
		R^2	0.60 (0.65*)	0.83 (0.83*)	0.85
		N	1638	1009	1303
	2016	Slope	0.88 (0.76*)	0.79 (0.77*)	0.82
		R^2	0.76 (0.79*)	0.84 (0.84*)	0.71
		N	1645	2010	1152
Wheat	2014–15	Slope	0.67	0.79	0.95
		R^2	0.73	0.85	0.89
		N	2051	1571	1671
	2015–16	Slope	0.59	0.76	0.81
		R^2	0.72	0.88	0.86
		N	2746	1644	1375
	2016–17	Slope	0.68	0.72	0.83
		R^2	0.68	0.82	0.88
		N	2659	614	1249

*Rice EBC without considering the water storage heat.

Accepted for publication in *Journal of Applied Meteorology and Climatology*. DOI 10.1175/JAMC-D-20-0233.1.

Table 5. Review of the eddy covariance-based total seasonal evapotranspiration (*ET*) (ET_{total}, mm), average seasonal daily *ET* (ET_{ave}, mm d^{-1}), mean growing season temperature (T_{ave}, °C), mean growing season vapor pressure deficit (*VPD*, kPa), mean growing season precipitation (P_{ave}, mm) and the maximum leaf area index (LAI_{max}, m^2 m^{-2}) in different regions for rice and wheat fields.

Crop	Location	Period	Climate	ET_{total}	ET_{ave}	T_{ave}	*VPD*	P_{ave}	LAI_{max}	Reference
Rice	Jiangsu, China (32°45’N, 120°28’E)	Jun–Nov, 2014–2017	Temperate	473	3.6	22	0.5	1025	5.4	This study
	Jiangsu, China (31°15’N, 120°57’E)	Jun–Oct, 2014	Temperate	470	3.1	16	–	1097	–	*Liu et al.* (2018)
	Kanto plain, Japan (36°03′N, 140°01′E)	May–Aug, 2002–2014	Temperate	419	3.5	22	0.6	1477	–	*Ikawa et al.* (2017)
	Rio Grande do Sul, Brazil (29°44’S, 53°08’W)	Nov–Apr, 2003–2004	Temperate	429	3.3	27	0.6	477	4.6	*Timm et al.* (2014)
	Heilongjiang, China (47°35’N, 133°31’E)	May–Oct, 2005–2006	Boreal	488	2.8	12	0.8	464	5.8	*Zhao et al.* (2008)
	Laguna, Philippines (14°8’N, 121°15’E)	May–Sep, 2008–2009	Tropical	496	4.0	28	0.8	1198	6.7	*Alberto et al.* (2011)
	Laguna, Philippines (14°08’N, 121°15’E; (14°18’N, 120°15’E)	Jan–May, 2011–2012	Tropical	499	4.2	27	–	409	4.1	*Alberto et al.* (2014)
Wheat	Jiangsu, China (32°45’N, 120°28’E)	Dec–May, 2014–2017	Temperate	387	2.4	12	0.3	298	2.7	This study

Accepted for publication in *Journal of Applied Meteorology and Climatology*. DOI 10.1175/JAMC-D-20-0233.1.

Beijing, China (39°37’N, 116°26’E)	Oct–Jun, 2007–2009	Arid	417	1.7	12	–	540	–	*Zhang et al.* (2013)
Shandong, China (36°39’N, 116°03’E)	Oct–May, 2005–2008	Arid	401	–	11	0.6	131	4.9	*Lei and Yang* (2010)
Gansu, China (42°02′N, 116°16′E)	Apr–Sep, 2009–2011	Arid	213	1.5	15	0.8	254	–	*Yang et al.* (2019)

Accepted for publication in *Journal of Applied Meteorology and Climatology*. DOI 10.1175/JAMC-D-20-0233.1.

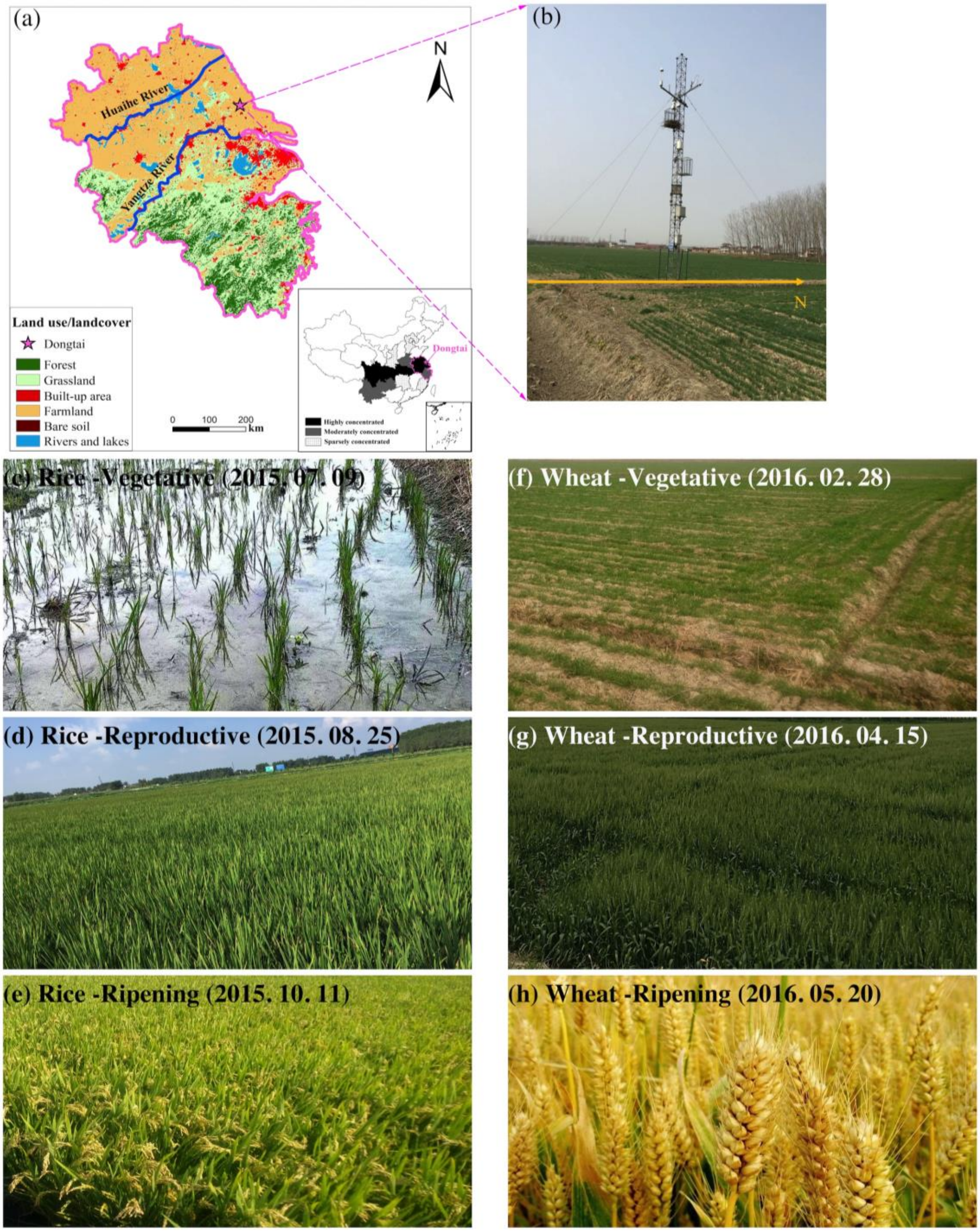

Figure 1. (a) Map showing the location of the Dongtai County study site (pink star) within eastern China, with the inset map showing the rice–wheat rotation area in China. (b) The 10 m observation tower (6 March 2016) with wheat (N = north). (c–h) The main growth stages (Table 1; vegetative, reproductive and ripening) of the (c–e) rice paddies and (f–h) wheat fields.

Accepted for publication in *Journal of Applied Meteorology and Climatology*. DOI 10.1175/JAMC-D-20-0233.1.

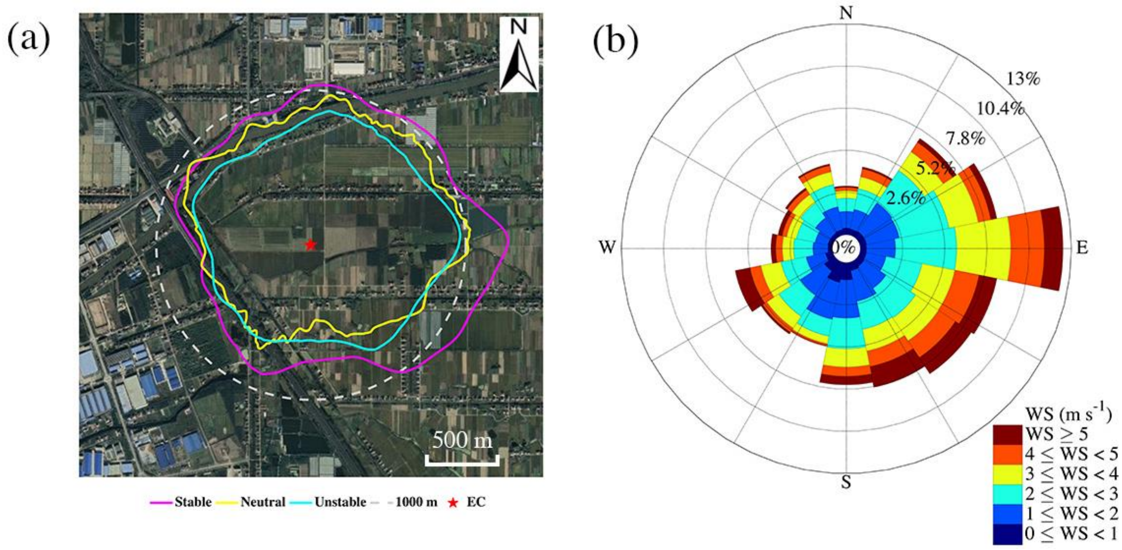

Figure 2. Climatology (2014–17) based on 10 m observations (red star): (a) eddy covariance 90% footprint with stability; and (b) wind rose. The background in (a) is from Google Earth on 6 February 2016.

Accepted for publication in *Journal of Applied Meteorology and Climatology*. DOI 10.1175/JAMC-D-20-0233.1.

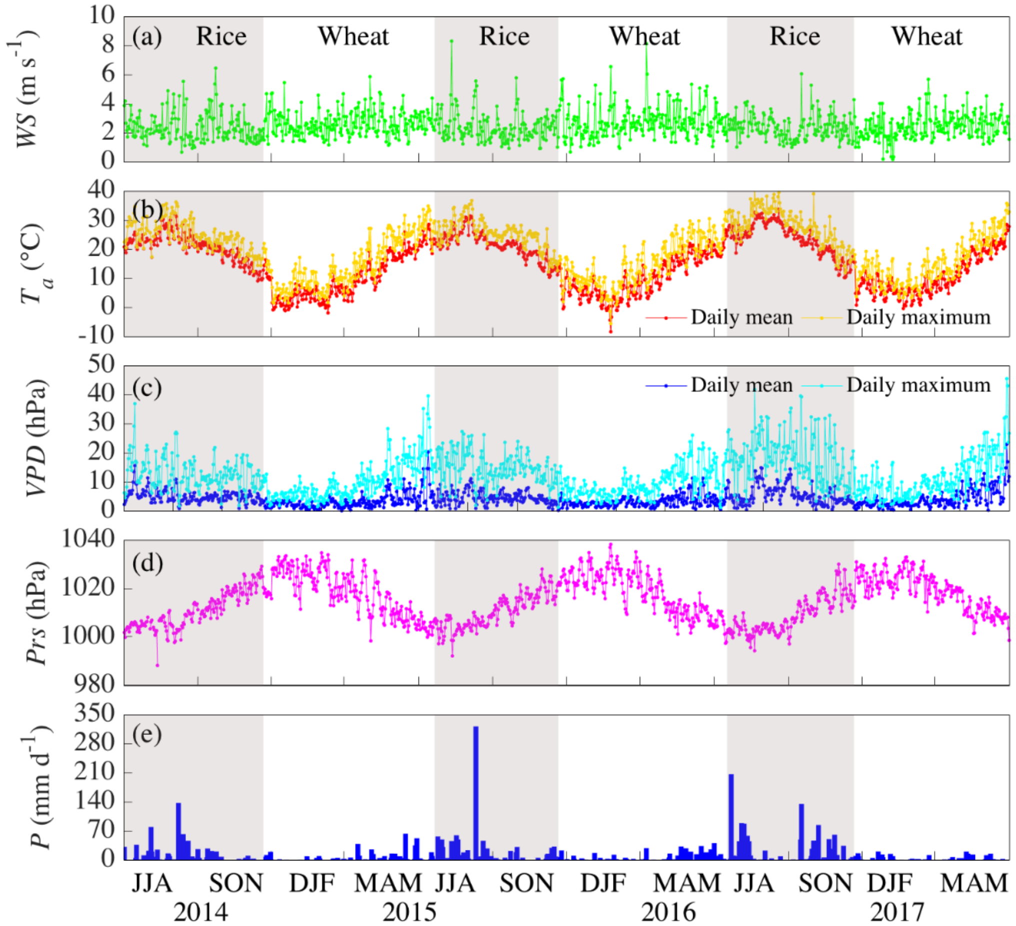

Figure 3. (a) Daily mean wind speed (*WS*), (b) daily mean and maximum air temperature (T_a), (c) daily mean and maximum vapor pressure deficit (*VPD*), (d) daily mean station pressure (P_{rs}), and (e) daily cumulative precipitation (*P*) for 2014–17.

Accepted for publication in *Journal of Applied Meteorology and Climatology*. DOI 10.1175/JAMC-D-20-0233.1.

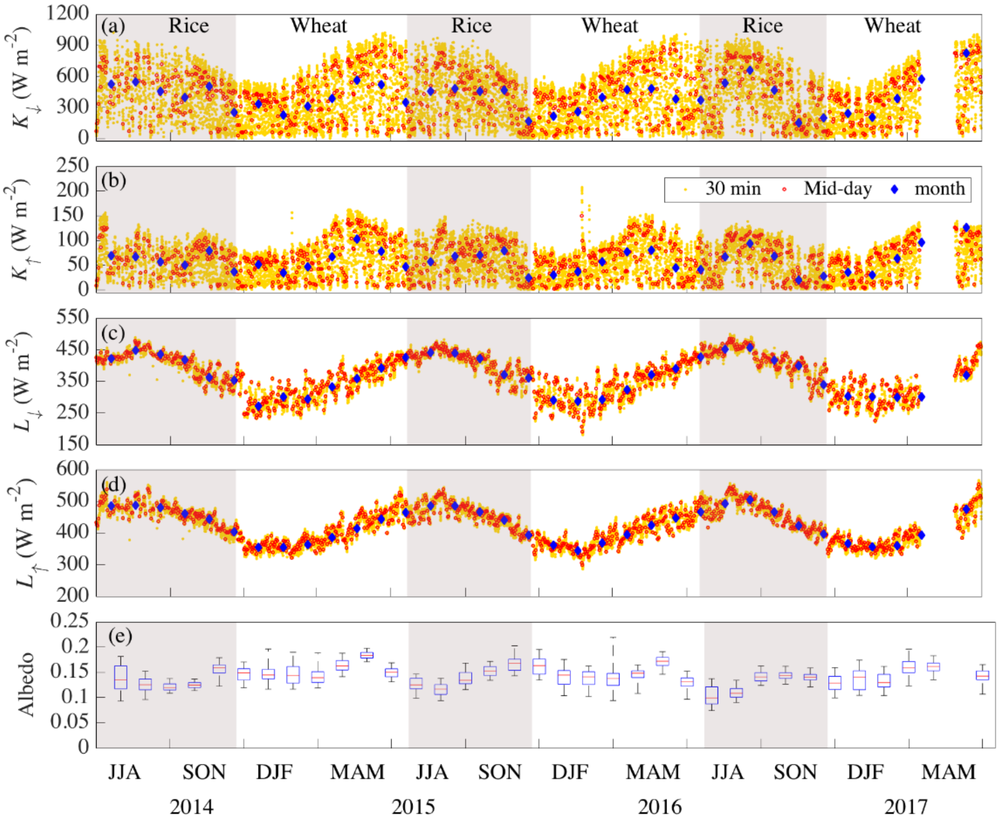

Figure 4. Observed 30 min (yellow dots), midday (10:00–16:00 LST; red circles) and monthly (blue diamonds) median fluxes of (a) incoming shortwave radiation ($K_{\downarrow}$), (b) outgoing shortwave radiation ($K_{\uparrow}$), (c) incoming longwave radiation ($L_{\downarrow}$), and (d) outgoing longwave radiation ($L_{\uparrow}$). (e) Boxplots (25th, 50th and 75th percentiles), with 10th and 90th percentile whiskers, for monthly surface albedo.

Accepted for publication in *Journal of Applied Meteorology and Climatology*. DOI 10.1175/JAMC-D-20-0233.1.

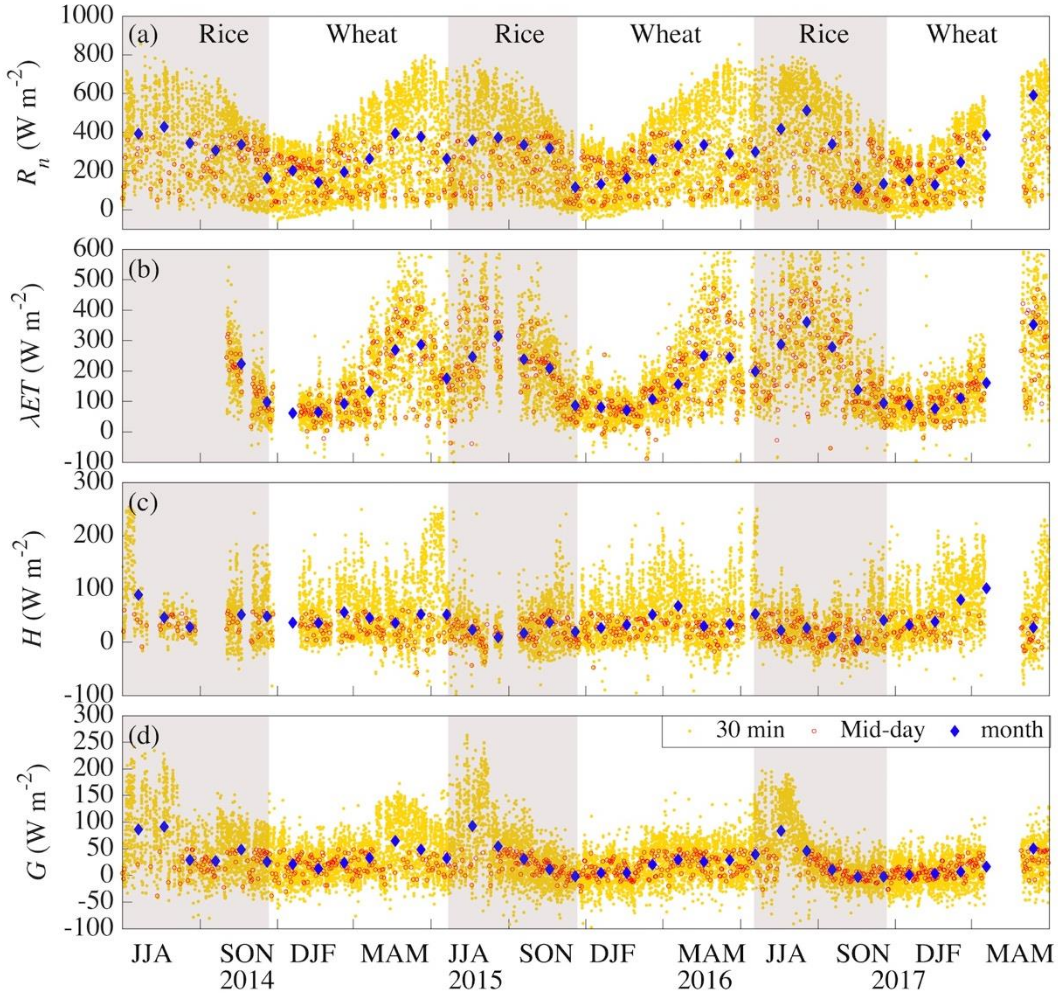

Figure 5. As in Figure 4, but for (a) net radiation (R_n), (b) turbulent latent heat flux (λET), (c) turbulent sensible heat flux (H), and (d) soil heat flux (G).

Accepted for publication in *Journal of Applied Meteorology and Climatology*. DOI 10.1175/JAMC-D-20-0233.1.

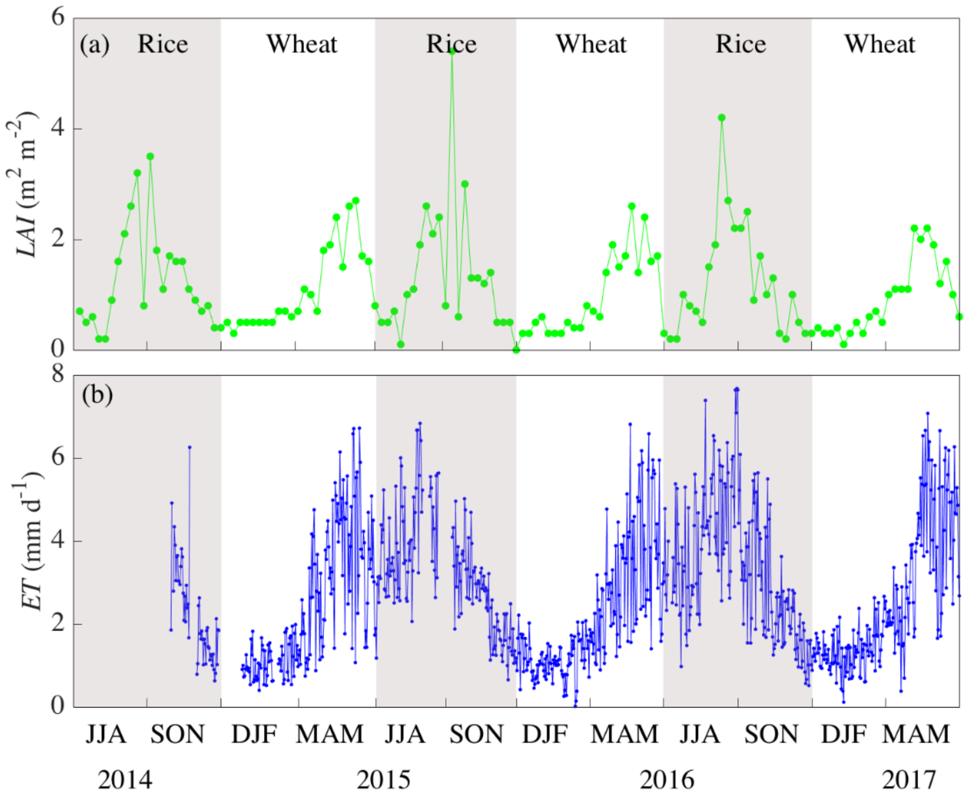

Figure 6. Seasonal variations in 8-day leaf area index (*LAI*) and daily total evapotranspiration (*ET*) for the 2014–17 cropping periods over the rice–wheat rotation.

Accepted for publication in *Journal of Applied Meteorology and Climatology*. DOI 10.1175/JAMC-D-20-0233.1.

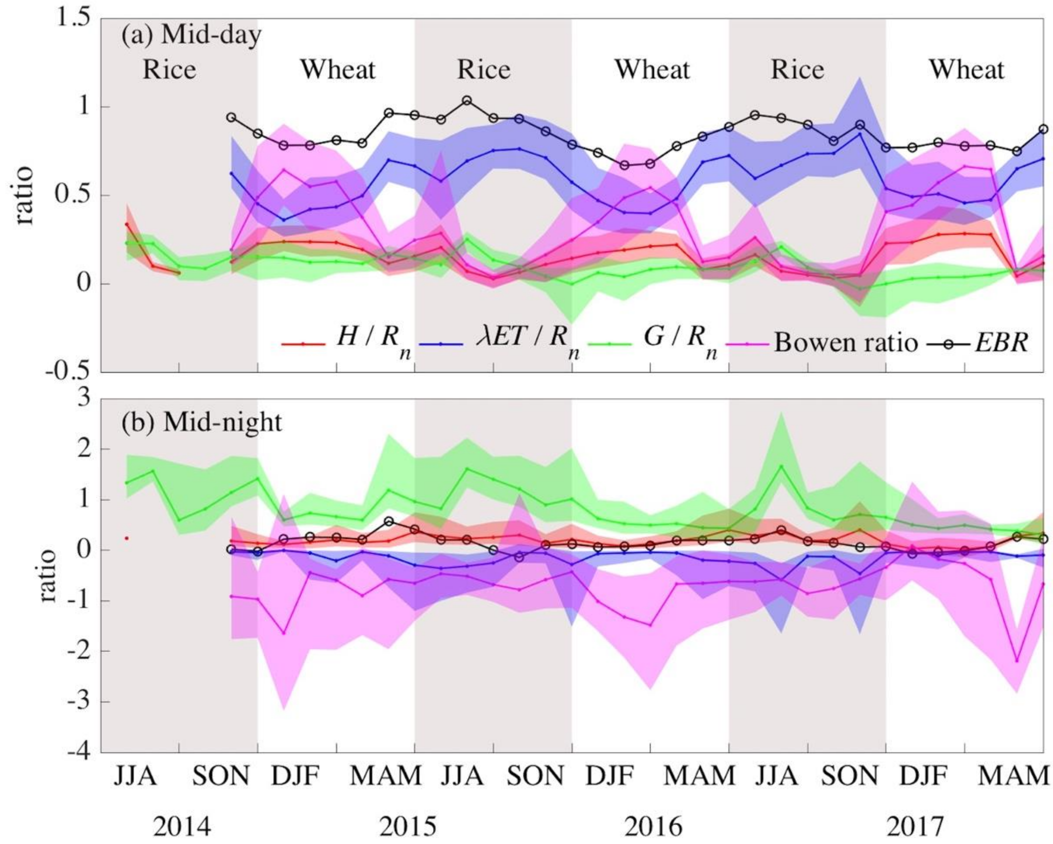

Figure 7. Variations of the monthly median (line) and interquartile range (shaded; between 1 June 2014 and 31 May 2017) ratios of sensible heat flux, latent heat flux and soil heat flux to net radiation, and the Bowen ratio (sensible to latent heat fluxes) during part of the (a) midday period (10:00–16:00 LST) and (b) midnight period (22:00–04:00 LST).

Accepted for publication in *Journal of Applied Meteorology and Climatology*. DOI 10.1175/JAMC-D-20-0233.1.